Extended State in a Localized Continuum

Wei Wang,* Xulong Wang,* and Guancong Ma†
Department of Physics, Hong Kong Baptist University, Kowloon Tong, Hong Kong, China

(Received 7 July 2022; accepted 5 December 2022; published 23 December 2022)

Bound state in a continuum (BIC) is a spatially confined resonance with its energy embedded in a continuous spectrum of propagative modes, yet their coupling is prohibited. In this Letter, we report the discovery of a generic non-Hermitian phenomenon that we call an "extended state in a localized continuum" (ELC). As the name suggests, the ELC is the inversion of the BIC—a single extended state embedded in a continuous spectrum entirely consisting of localized modes, and its emergence rests in the interplay between the BIC and the non-Hermitian skin effect (NHSE). Herein, the BIC is a zero-energy corner mode that spectrally overlaps with a bulk band in a Hermitian kagome lattice. The ELC emerges with the introduction of the NHSE in a particular way, such that it turns all the bulk states into corner skin modes and simultaneously delocalizes the corner mode. We experimentally realize the ELC using an active mechanical lattice. Our findings not only demonstrate the rich potential of the NHSE but may also spark new wave-based applications.

DOI: 10.1103/PhysRevLett.129.264301

Introduction.—Bound state in a continuum (BIC) is a localized state that spatially and spectrally overlaps with a continuum of extended states but does not hybridize with any of them [1,2]. BICs ubiquitously appear in a wide range of physical systems, including quantum dots [3–5], and classical waves [6–13]. They have led to high-performance applications, such as nonlinear optics [14–16], sensing [17–19], filtering [20], and lasers [21–24]. The unique characteristics of BICs are enabled by either incompatible symmetries or by accidental destructive interferences among radiative or hybridization channels [2]. In particular, by virtue of Hilbert-space separability or geometric symmetry, topological or defect modes can be tuned to spectrally overlap with a band of extended bulk modes while maintaining their localized characteristics, thus becoming BICs [25–28].

In a separate realm, the development of non-Hermitian formalism has fundamentally changed our understanding of open systems [29,30]. It has not only brought about new analytical tools, which enabled a kaleidoscope of revolutionary applications in optics, photonics, and classical waves [31,32], but also broken new grounds for topological physics [33,34]. Specifically, the complex spectrum gives rise to spectral topology [35]. An important consequence is the non-Hermitian skin effect (NHSE) [36–40], which causes the bulk states in an open lattice to become skin modes localized at boundaries. The NHSE has been realized in classical wave systems [41–44], electric circuits [45], and quantum walks [46,47]. Recently, it was discovered that the NHSE can also modify the wave functions of topological modes by delocalization [48–51] or by imposing further spatial confinement [51–53].

In this Letter, we report the discovery and experimental realization of a new phenomenon, named "an extended state in a localized continuum" (ELC). The emergence of the ELC rests in the confluence of the BIC and the NHSE. Our system is based on a 2D kagome rhombic lattice possessing a BIC—a corner mode pinned at zero energy [54–58] and embedded in a continuum of extended bulk modes. By introducing specific nonreciprocal hopping, the NHSE counters the spatial exponential decay of the zero mode and delocalizes it into a fully extended state. The extended zero mode remains spectrally embedded in the continuum band, in which all modes are skin modes collapsing toward a corner due to the NHSE. In other words, the ELC is a BIC inverted by the NHSE.

Theoretical model.—Figure 1(a) shows a non-Hermitian kagome lattice. The Hamiltonian under the periodic boundary conditions (PBCs) reads

$$h(\boldsymbol{k}) = \begin{bmatrix} 0 & t_1+t_2e^{-i\boldsymbol{k}\cdot\boldsymbol{a_1}} & t_1+t_2e^{-i\boldsymbol{k}\cdot\boldsymbol{a_2}} \\ (t_1+\varepsilon_{12})+t_2e^{i\boldsymbol{k}\cdot\boldsymbol{a_1}} & 0 & t_1+t_2e^{-i\boldsymbol{k}\cdot(\boldsymbol{a_2}-\boldsymbol{a_1})} \\ (t_1+\varepsilon_{13})+t_2e^{i\boldsymbol{k}\cdot\boldsymbol{a_2}} & t_1+t_2e^{i\boldsymbol{k}\cdot(\boldsymbol{a_2}-\boldsymbol{a_1})} & 0 \end{bmatrix}, \tag{1}$$

where $\boldsymbol{k}=(k_x,k_y)$ is the Bloch wave vector, $\boldsymbol{a_1}=(1,0)$ and $\boldsymbol{a_2}=(1/2,\sqrt{3}/2)$ are the primitive vectors, t_1 and t_2 are the hopping coefficients, ε_{12} and ε_{13} are the nonreciprocal hopping coefficients between sites 1, 2 and sites 1, 3. When $\varepsilon_{12}=\varepsilon_{13}=0$, Eq. (1) is Hermitian and the spectrum under the PBC is shown in Fig. 1(b), in which we set $t_1=-0.73$ and $t_2=-0.97$. Model (1) possesses C_{3v} and a

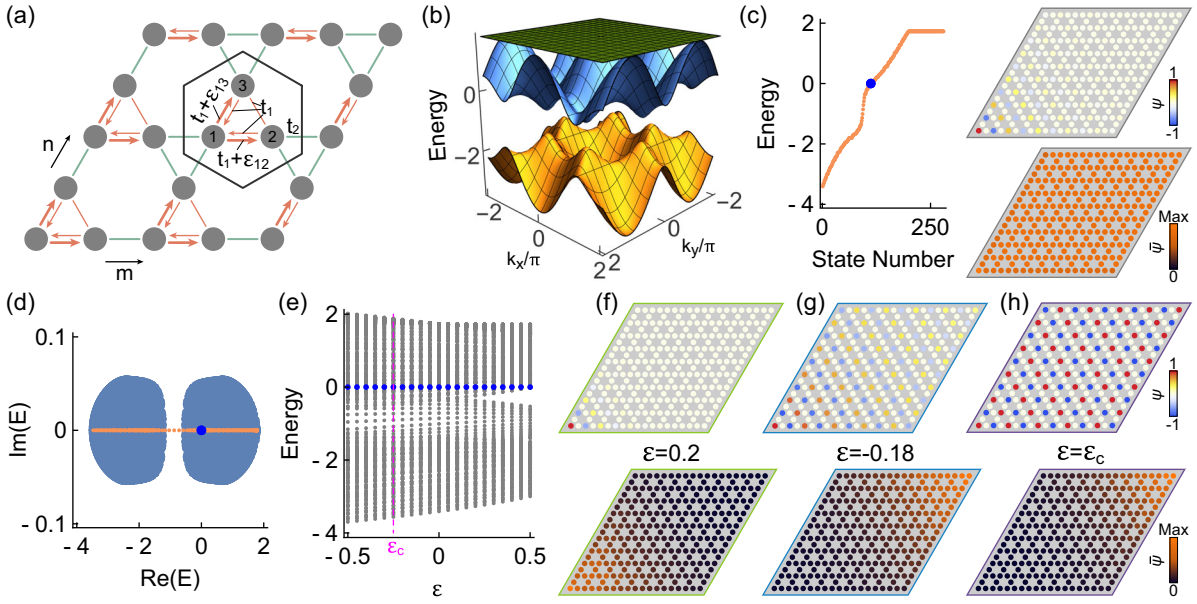

FIG. 1. (a) The schematic of a non-Hermitian kagome lattice. The black hexagon encircles a unit cell. (b) The spectrum of a Hermitian kagome lattice under the PBC. (c) Left panel: the OBC spectrum of a Hermitian rhombic lattice. The blue dot denotes the zero mode. Right panels: the wave function of the zero mode and the averaged distribution of the bulk modes in the second bulk band. (d) The PBC (light blue) and OBC (orange) spectra of the non-Hermitian kagome lattice. (e) The OBC spectra of the non-Hermitian rhombic lattice and its dependence on ε. (f)–(h) The wave function of the zero mode (upper panels) and the averaged wave function of the bulk modes (bottom panels) at (f) $\varepsilon = 0.2$, (g) $\varepsilon = -0.18$, and (h) $\varepsilon = \varepsilon_c = -0.24$.

generalized chiral symmetry [55]. Under an open boundary condition (OBC), an equilateral-rhombic lattice (280 sites) sustains a zero mode [54], as shown in Fig. 1(c). The wave function of the zero mode is analytically solvable

$$|\psi^H_{\text{zero}}\rangle = \mathcal{N} \sum_{(m,n)} (-t_1/t_2)^{m+n} c^\dagger_{1,(m,n)} |0\rangle, \tag{2}$$

where $|0\rangle$ is a zero vector, $c^\dagger_{1,(m,n)}$ is a creation operator at site 1 in the unit cell index by (m,n), with the cell at the lower-left corner as (0,0), and $\mathcal{N}$ is a normalization factor. From Eq. (2) it is readily apparent that the wave function of the zero mode is nonzero only at sites 1 and is exponentially localized at the lower-left corner. Moreover, the zero mode is spectrally embedded in a bulk band. Figure 1(c) also plots the averaged distribution of all bulk modes in the second band, i.e., $\bar{\psi} = (1/N)\sum_i^N |\psi_i|^2$, where N is the number of the corresponding bulk modes. These observations are a clear indication that the zero mode is a BIC [55].

The system is non-Hermitian when ε_{12} and (or) ε_{13} in Eq. (1) are nonzero. We choose a constant nonreciprocal hopping, that is $\varepsilon_{12} = \varepsilon_{13} = \varepsilon$. In this case, the PBC spectrum is complex and it forms spectral areas in the complex plane, as shown in Fig. 1(d) for $\varepsilon = -0.1$. Owing to the nonreciprocal hopping, the NHSE emerges and collapses the bulk modes toward the boundaries (corners) under the OBC. The OBC spectra of the rhombic lattice are plotted in Fig. 1(e) as a function of ε. Two important observations are made: the spectrum remains real due to the pseudo-Hermiticity of the OBC Hamiltonian [59], and the zero mode exists for all ε. When $\varepsilon \neq 0$, the C_3 and the reflection symmetry that maps site 1 to site 2 and site 1 to site 3 are broken. However, the reflection symmetry mapping site 2 to site 3 remains intact and the generalized chiral symmetry is also preserved. The wave function of the zero mode in the non-Hermitian rhombic lattice is given by

$$|\psi^{NH}_{\text{zero}}\rangle = \mathcal{N}' \sum_{(m,n)} [-(t_1+\varepsilon)/t_2]^{m+n} c^\dagger_{1,(m,n)} |0\rangle. \tag{3}$$

Clearly, it is tunable by the non-Hermitian parameter ε, as shown in the upper panels of Figs. 1(f)–1(h). For a positive ε, $|\psi^{NH}_{\text{zero}}\rangle$ is even more localized with a shorter decay length compared to $|\psi^H_{\text{zero}}\rangle$. In this case, all bulk modes are skin modes localized at the lower-left corner [Fig. 1(f)]. When $\varepsilon < 0$, the bulk modes congregate at the upper-right corner, yet the zero mode is seen to delocalize [Fig. 1(g)]. It becomes decay free across the entire lattice at a critical value $\varepsilon_c = t_2 - t_1 = -0.24$ [Fig. 1(h)]. (There exists another critical value at $\varepsilon'_c = -t_2 - t_1 = 1.7$ [60]). Note that the OBC spectrum remains entirely real, and the zero mode is embedded in the continuum band. Thus, we have arrived at a new phenomenon that a band of corner-localized skin modes forms a continuum, in which a single fully extended zero mode is embedded [Fig. 1(h)]. In other

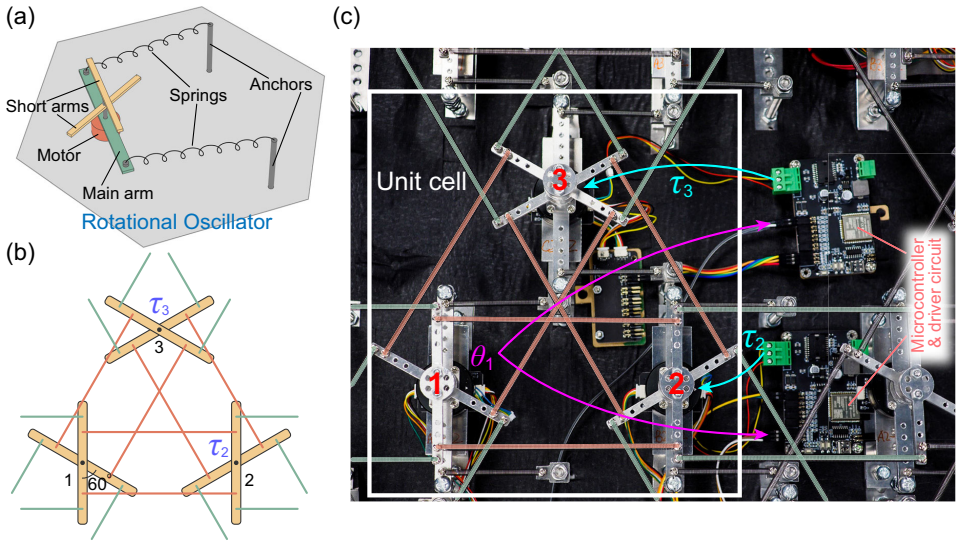

FIG. 2. (a) The schematic drawing of the rotational resonator, whose resonance plays the role of the on-site orbital. (b) The schematic drawing of a unit cell of the non-Hermitian kagome lattice. Only the short arms supporting the connections between neighboring sites are shown. $\tau_2(t)$ and $\tau_3(t)$ are the instantaneous torques applied on site 2 and site 3. (c) A photo of the mechanical lattice. The tension springs realizing the hoppings t_1 and t_2 are colored according to (b). $\theta_1(t)$ is the instantaneous angular displacement of site 1. The white box marks the unit cell.

words, the BIC is turned into an ELC when introducing the NHSE.

Experiments.—We use a lattice of rotational oscillators to realize the EIC. A typical oscillator is shown in Fig. 2(a), which consists of a brushless dc motor (LDPOWER 2804) with a 124-mm metallic arm anchored by two tensioned springs such that there is only one rotational degree of freedom. The main arm can accommodate additional weight loading for adjusting the moment of inertia, by which the resonant frequency is tuned to 13 Hz. (This is the frequency for the "zero energy" in the theoretical model.) Stacked on top of the main arm are two additional arms, on which springs that connect neighboring sites are attached, such that the kagome lattice is built, as shown in Figs. 2(b) and 2(c). To realize the nonreciprocal hopping, electronics [Fig. 2(c)] are used to measure the instantaneous angular displacement $\theta_1(t)$ at all sites 1 in real time. The results are used as feedback to generate instantaneous torques at sites 2 and 3 in the same unit cell, $\tau_2(t) = \tau_3(t) = \alpha\theta_1(t)$, where α is a constant that tunes the magnitude of the nonreciprocal hopping. More details about the experimental setup are presented in Ref. [60].

The experimental lattice has 65 oscillators. We first set $\varepsilon = 0$ and excite a single oscillator in the bulk with a signal covering 6–20 Hz. The response spectrum shows a dip at 12.3 Hz which indicates a band gap, separating two bulk bands [Fig. 3(a)]. We then apply actuation on the oscillator at the lower-left corner and the corresponding response spectrum is displayed as the orange curve. A sharp peak is seen at 13.3 Hz, overlapping with the higher bulk band. The finite linewidth of the peak is due to dissipation in the lattice. The quality factor can be much higher if the dissipation is reduced. The steady-state vibration profile measured at all sites at this frequency is clearly localized at the lower-left corner [Fig. 3(f)], which is in good agreement with the response profile computed using Green's function [Fig. 3(c)]. This realizes the BIC in the Hermitian kagome lattice.

We next switch on the nonreciprocal hopping and set $\varepsilon = -0.26$ (retrieved value, close to the critical value ε_c). The NHSE is observed, as demonstrated in the Supplemental Material video [60]. The response spectra for the excitation in the bulk and at the lower-left corner are shown in Fig. 3(b). Both spectra are similar to their Hermitian counterparts. However, when excited at the lower-left corner, the vibration profile at 13.3 Hz is no longer localized at the corner, but occupies the entire lattice [Fig. 3(g)]. This signifies that the zero mode is entirely delocalized and has become an extended mode. There is a slight drop in vibrational magnitudes away from the source, which is attributed to the inevitable presence of dissipation in the lattice. The dissipation also broadens the responses of all modes, such that the monochromatic excitation at 13.3 Hz can also weakly excite nearby bulk modes. These modes also contribute to the overall vibration profile that is shown in Fig. 3(g). This is also verified by the good agreement between the measured and the theoretically calculated results [Fig. 3(d)], in which the dissipation is accounted for in Green's function. We also show in Ref. [60], that upon decreasing the dissipation, it is indeed possible to excite only the extended zero mode with the excitation at the lower-left corner.

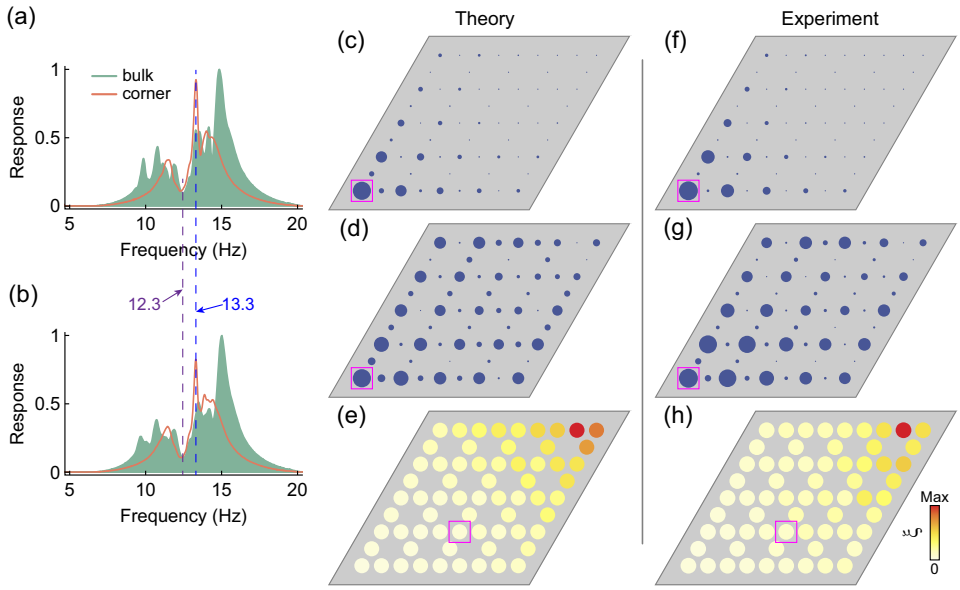

FIG. 3. (a) and (b) The response spectra of the 65-site rhombic lattice with the excitation placed inside the bulk and at the lower-left corner when (a) $\varepsilon = 0$ and (b) $\varepsilon = -0.26$. (c) and (d) The theoretical and (f) and (g) experimental steady-state response fields when the lattice is excited at the lower-left corner at 13.3 Hz. The results in (c) and (f) correspond to the Hermitian case with $\varepsilon = 0$, and the results in (d) and (g) are at $\varepsilon = -0.26$. (e) The theoretical and (h) experimental response ratio of the non-Hermitian and Hermitian lattices. The magenta box in (c)–(h) marks the position of the source. The size of the circles in (c), (d), (f), and (g) represents the response magnitude.

Next, we place a single source in the bulk and away from the mirror axis [Fig. 4(b)] to excite both the symmetric and antisymmetric skin modes. The spectral sum of the responses at each site is then obtained

$$P_{\nu,(m,n)} = \int_{f_1}^{f_2} |A_{\nu,(m,n)}(f)|^2 df, \tag{4}$$

where $A_{\nu,(m,n)}(f)$ is the response of the site ν of the unit cell (m,n) at frequency f, with $\nu = 1, 2, 3$, and $f_1 = 6$ Hz and $f_2 = 20$ Hz. The response ratio between the non-Hermitian and Hermitian lattices $\xi_{\nu,(m,n)} = P^{NH}_{\nu,(m,n)}/P^{H}_{\nu,(m,n)}$ is shown in Figs. 3(h). Figure 3(e) shows the theoretical result. These results clearly show that when the nonreciprocal hopping is in effect, all bulk modes become skin modes that localize at the upper-right corner. From these experimental data, it becomes clear that we have successfully verified the existence of the ELC in our mechanical lattice.

Discussion and conclusion.—The ELC is the phenomenological inversion of the BIC. It is the unique consequence of the interplay between the BIC and the NHSE. The exponential decay of the corner mode is exactly countered by the spatial amplification caused by the NHSE [49], resulting in an extended state. Meanwhile, the bulk modes that form the continuum band become corner-localized skin modes (the localization characteristic is more evident in a sufficiently large lattice). Unlike the BIC, the ELC is one of the non-Hermitian eigenmodes, which are generically skewed and follow biorthogonality [63], that is $\langle \psi_i^L | \psi_j^R \rangle = \delta_{ij}$, where i, j are the mode indices, ψ_i^L and ψ_j^R are bilinearly normalized left and right eigenvectors [64,65]. The biorthogonal inner products of the ELC and all the other skin modes, denoted $\chi^{LR} \equiv \langle \psi_i^L | \psi_{\text{zero}}^{NH,R} \rangle$, are indeed vanishing as shown in Fig. 4(a). This means that the stable existence of the ELC is a consequence of biorthogonality—an exclusively non-Hermitian property. The inner products using only the right eigenvectors, denoted $\chi^{RR} \equiv \langle \psi_i^R | \psi_{\text{zero}}^{NH,R} \rangle$, can indeed be nonzero [Fig. 4(b)]. However, intriguingly, a significant portion of the bulk modes still gives a vanishing χ^{RR}. Futher examination reveals that the corresponding modes are all antisymmetric about the mirror axis of the rhombic lattice, and they are incompatible with the extended zero mode that is symmetric. In other words, instead of being a generic phenomenon, the vanishing of χ^{RR} relies on the specific spatial symmetry C_s of the OBC lattice.

The forms of the ELC are diverse and tailorable. For example, by using a triangular lattice, the ELC is an extended state in a continuum of edge-localized skin modes [60]. It is also straightforward to realize an ELC in different types of lattices. An additional example based on a 2D non-Hermitian Su-Schrieffer-Heeger lattice is presented in Ref. [60] where the Hermitian BIC is also a topological mode. These desirable characteristics mean the ELC can potentially be tailored to adapt to different application scenarios. Because the physical mechanisms for the BICs and the NHSE are universal, this phenomenon can emerge in other types of systems, such as photonics, electromagnetism, acoustics, and in the continuous models which are out of the tight-binding descriptions. Recent work showing

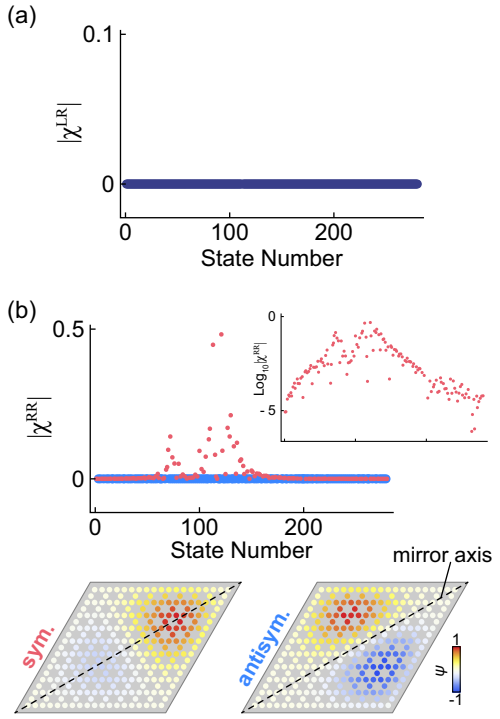

FIG. 4. (a) The biorthogonal inner product $|\chi^{LR}|$ of the extended zero mode and all other skin modes. (b) Upper panel: the results of $|\chi^{RR}|$ between the extended zero mode and all other skin modes. The zero and nonzero values are shown in pink and light blue, respectively. The inset shows the nonzero $|\chi^{RR}|$ in a semilogarithm plot (base 10). Bottom panels: the representative symmetric and antisymmetric skin modes.

the possibility of realizing nonreciprocity by loss [66] suggests the potential of obtaining ELC in completely passive systems.

We remark that, even in the presence of the NHSE, in 1D lattices, it remains possible for a small number of bulk modes to be extended [43,67]. Such states owe their existence to the bipolar NHSE, which occurs when the energy of an OBC eigenstate exactly coincides with the PBC spectrum in the complex plane. Hence, the OBC bulk modes can still converge to the PBC eigenmodes. However, the very mechanism for such a "Bloch-wave-like" state to exist also prevents it from overlapping with other skin modes. Thus, it cannot become an ELC.

In summary, the ELC demonstrated here exemplifies the rich possibilities that lie within the confluence of generic wave physics and non-Hermitian physics. We envisage the ELC to bring intriguing twists to wave-based applications, especially BIC-based devices. For instance, quasi-BIC lasers [21,68] can benefit from the extended mode profile of the ELC, such that surface emission may be attainable. BIC-based sensors [18,19] can also take advantage of the increased detection area, thereby boosting their efficiency. The ELC may also boost the energy capacity for gapless photonic crystal fibers relying on BIC [69].

This work was supported by the National Natural Science Foundation of China (11922416) and the Hong Kong Research Grants Council (RFS2223-2S01, 12302420, 12300419, 12301822) and the National Key R&D Program of China (2022YFA1404400).

*These authors contributed equally to this work.
†phgcma@hkbu.edu.hk

[1] J. Von Neumann and E. Wigner, Über Merkwürdige Diskrete Eigenwerte, Phys. Z. **30**, 465 (1929).
[2] C. W. Hsu, B. Zhen, A. D. Stone, J. D. Joannopoulos, and M. Soljačić, Bound states in the continuum, Nat. Rev. Mater. **1**, 16048 (2016).
[3] M. L. de Guevara, F. Claro, and P. A. Orellana, Ghost Fano resonance in a double quantum dot molecule attached to leads, Phys. Rev. B **67**, 195335 (2003).
[4] M. L. Ladrón de Guevara and P. A. Orellana, Electronic transport through a parallel-coupled triple quantum dot molecule: Fano resonances and bound states in the continuum, Phys. Rev. B **73**, 205303 (2006).
[5] K.-K. Voo and C. S. Chu, Localized states in continuum in low-dimensional systems, Phys. Rev. B **74**, 155306 (2006).
[6] D. C. Marinica, A. G. Borisov, and S. V. Shabanov, Bound States in the Continuum in Photonics, Phys. Rev. Lett. **100**, 183902 (2008).
[7] Y. Plotnik, O. Peleg, F. Dreisow, M. Heinrich, S. Nolte, A. Szameit, and M. Segev, Experimental Observation of Optical Bound States in the Continuum, Phys. Rev. Lett. **107**, 183901 (2011).
[8] S. Hein, W. Koch, and L. Nannen, Trapped modes and Fano resonances in two-dimensional acoustical duct–cavity systems, J. Fluid Mech. **692**, 257 (2012).
[9] C. W. Hsu, B. Zhen, J. Lee, S.-L. Chua, S. G. Johnson, J. D. Joannopoulos, and M. Soljačić, Observation of trapped light within the radiation continuum, Nature (London) **499**, 188 (2013).
[10] C. Huang *et al.*, Ultrafast control of vortex microlasers, Science **367**, 1018 (2020).
[11] S. Huang, T. Liu, Z. Zhou, X. Wang, J. Zhu, and Y. Li, Extreme Sound Confinement From Quasibound States in the Continuum, Phys. Rev. Appl. **14**, 021001 (2020).
[12] L. Huang, Y. K. Chiang, S. Huang, C. Shen, F. Deng, Y. Cheng, B. Jia, Y. Li, D. A. Powell, and A. E. Miroshnichenko, Sound trapping in an open resonator, Nat. Commun. **12**, 4819 (2021).
[13] L. Cao, Y. Zhu, Y. Xu, S.-W. Fan, Z. Yang, and B. Assouar, Elastic bound state in the continuum with perfect mode conversion, J. Mech. Phys. Solids **154**, 104502 (2021).
[14] L. Carletti, K. Koshelev, C. De Angelis, and Y. Kivshar, Giant Nonlinear Response at the Nanoscale Driven by Bound States in the Continuum, Phys. Rev. Lett. **121**, 033903 (2018).
[15] E. N. Bulgakov and A. F. Sadreev, Robust bound state in the continuum in a nonlinear microcavity embedded in a photonic crystal waveguide, Opt. Lett. **39**, 5212 (2014).
[16] S. D. Krasikov, A. A. Bogdanov, and I. V. Iorsh, Nonlinear bound states in the continuum of a one-dimensional photonic crystal slab, Phys. Rev. B **97**, 224309 (2018).

[17] A. A. Yanik, A. E. Cetin, M. Huang, A. Artar, S. H. Mousavi, A. Khanikaev, J. H. Connor, G. Shvets, and H. Altug, Seeing protein monolayers with naked eye through plasmonic Fano resonances, Proc. Natl. Acad. Sci. U.S.A. **108**, 11784 (2011).
[18] Y. Liu, W. Zhou, and Y. Sun, Optical refractive index sensing based on high-Q bound states in the continuum in free-space coupled photonic crystal slabs, Sensors **17**, 1861 (2017).
[19] S. Romano, G. Zito, S. N. L. Yépez, S. Cabrini, E. Penzo, G. Coppola, I. Rendina, and V. Mocellaark, Tuning the exponential sensitivity of a bound-state-in-continuum optical sensor, Opt. Express **27**, 18776 (2019).
[20] J. M. Foley, S. M. Young, and J. D. Phillips, Symmetry-protected mode coupling near normal incidence for narrow-band transmission filtering in a dielectric grating, Phys. Rev. B **89**, 165111 (2014).
[21] A. Kodigala, T. Lepetit, Q. Gu, B. Bahari, Y. Fainman, and B. Kanté, Lasing action from photonic bound states in continuum, Nature (London) **541**, 196 (2017).
[22] Y. Song, N. Jiang, L. Liu, X. Hu, and J. Zi, Cherenkov Radiation from Photonic Bound States in the Continuum: Towards Compact Free-Electron Lasers, Phys. Rev. Appl. **10**, 064026 (2018).
[23] B. Midya and V. V. Konotop, Coherent-perfect-absorber and laser for bound states in a continuum, Opt. Lett. **43**, 607 (2018).
[24] Y. Yu, A. Sakanas, A. R. Zali, E. Semenova, K. Yvind, and J. Mørk, Ultra-coherent Fano laser based on a bound state in the continuum, Nat. Photonics **15**, 758 (2021).
[25] Y.-X. Xiao, G. Ma, Z.-Q. Zhang, and C. T. Chan, Topological Subspace-Induced Bound State in the Continuum, Phys. Rev. Lett. **118**, 166803 (2017).
[26] Z.-G. Chen, C. Xu, R. Al Jahdali, J. Mei, and Y. Wu, Corner states in a second-order acoustic topological insulator as bound states in the continuum, Phys. Rev. B **100**, 075120 (2019).
[27] Z.-G. Chen, L. Wang, G. Zhang, and G. Ma, Chiral Symmetry Breaking of Tight-Binding Models in Coupled Acoustic-Cavity Systems, Phys. Rev. Appl. **14**, 024023 (2020).
[28] Z.-G. Chen, W. Zhu, Y. Tan, L. Wang, and G. Ma, Acoustic Realization of a Four-Dimensional Higher-Order Chern Insulator and Boundary-Modes Engineering, Phys. Rev. X **11**, 011016 (2021).
[29] C. M. Bender, Making sense of non-Hermitian Hamiltonians, Rep. Prog. Phys. **70**, 947 (2007).
[30] Y. Ashida, Z. Gong, and M. Ueda, Non-Hermitian Physics, Adv. Phys. **69**, 249 (2020).
[31] L. Feng, R. El-Ganainy, and L. Ge, Non-Hermitian photonics based on parity–time symmetry, Nat. Photonics **11**, 752 (2017).
[32] Ş. K. Özdemir, S. Rotter, F. Nori, and L. Yang, Parity–time symmetry and exceptional points in photonics, Nat. Mater. **18**, 783 (2019).
[33] E. J. Bergholtz, J. C. Budich, and F. K. Kunst, Exceptional topology of non-Hermitian systems, Rev. Mod. Phys. **93**, 015005 (2021).
[34] K. Ding, C. Fang, and G. Ma, Non-Hermitian topology and exceptional-point geometries, Nat. Rev. Phys. **4**, 745 (2022).
[35] K. Kawabata, K. Shiozaki, M. Ueda, and M. Sato, Symmetry and Topology in Non-Hermitian Physics, Phys. Rev. X **9**, 041015 (2019).
[36] S. Yao and Z. Wang, Edge States and Topological Invariants of Non-Hermitian Systems, Phys. Rev. Lett. **121**, 086803 (2018).
[37] F. K. Kunst, E. Edvardsson, J. C. Budich, and E. J. Bergholtz, Biorthogonal Bulk-Boundary Correspondence in Non-Hermitian Systems, Phys. Rev. Lett. **121**, 026808 (2018).
[38] K. Yokomizo and S. Murakami, Non-Bloch Band Theory of Non-Hermitian Systems, Phys. Rev. Lett. **123**, 066404 (2019).
[39] N. Okuma, K. Kawabata, K. Shiozaki, and M. Sato, Topological Origin of Non-Hermitian Skin Effects, Phys. Rev. Lett. **124**, 086801 (2020).
[40] K. Zhang, Z. Yang, and C. Fang, Correspondence between Winding Numbers and Skin Modes in Non-Hermitian Systems, Phys. Rev. Lett. **125**, 126402 (2020).
[41] A. Ghatak, M. Brandenbourger, J. van Wezel, and C. Coulais, Observation of non-Hermitian topology and its bulk–edge correspondence in an active mechanical metamaterial, Proc. Natl. Acad. Sci. U.S.A. **117**, 29561 (2020).
[42] S. Weidemann, M. Kremer, T. Helbig, T. Hofmann, A. Stegmaier, M. Greiter, R. Thomale, and A. Szameit, Topological funneling of light, Science **368**, 311 (2020).
[43] L. Zhang *et al.*, Acoustic non-Hermitian skin effect from twisted winding topology, Nat. Commun. **12**, 6297 (2021).
[44] X. Zhang, Y. Tian, J.-H. Jiang, M.-H. Lu, and Y.-F. Chen, Observation of higher-order non-Hermitian skin effect, Nat. Commun. **12**, 5377 (2021).
[45] T. Helbig, T. Hofmann, S. Imhof, M. Abdelghany, T. Kiessling, L. W. Molenkamp, C. H. Lee, A. Szameit, M. Greiter, and R. Thomale, Generalized bulk–boundary correspondence in non-Hermitian topolectrical circuits, Nat. Phys. **16**, 747 (2020).
[46] L. Xiao, T. Deng, K. Wang, G. Zhu, Z. Wang, W. Yi, and P. Xue, Non-Hermitian bulk–boundary correspondence in quantum dynamics, Nat. Phys. **16**, 761 (2020).
[47] L. Xiao, T. Deng, K. Wang, Z. Wang, W. Yi, and P. Xue, Observation of Non-Bloch Parity-Time Symmetry and Exceptional Points, Phys. Rev. Lett. **126**, 230402 (2021).
[48] S. Longhi, Non-Hermitian gauged topological laser arrays, Ann. Phys. (Amsterdam) **530**, 1800023 (2018).
[49] W. Zhu, W. X. Teo, L. Li, and J. Gong, Delocalization of topological edge states, Phys. Rev. B **103**, 195414 (2021).
[50] W. X. Teo, W. Zhu, and J. Gong, Tunable two-dimensional laser arrays with zero-phase locking, Phys. Rev. B **105**, L201402 (2022).
[51] W. Wang, X. Wang, and G. Ma, Non-Hermitian morphing of topological modes, Nature (London) **608**, 50 (2022).
[52] C. H. Lee, L. Li, and J. Gong, Hybrid Higher-Order Skin-Topological Modes in Nonreciprocal Systems, Phys. Rev. Lett. **123**, 016805 (2019).
[53] D. Zou, T. Chen, W. He, J. Bao, C. H. Lee, H. Sun, and X. Zhang, Observation of hybrid higher-order skin-topological effect in non-Hermitian topolectrical circuits, Nat. Commun. **12**, 7201 (2021).

[54] F. K. Kunst, G. van Miert, and E. J. Bergholtz, Lattice models with exactly solvable topological hinge and corner states, Phys. Rev. B **97**, 241405(R) (2018).
[55] X. Ni, M. Weiner, A. Alù, and A. B. Khanikaev, Observation of higher-order topological acoustic states protected by generalized chiral symmetry, Nat. Mater. **18**, 113 (2019).
[56] H. Xue, Y. Yang, F. Gao, Y. Chong, and B. Zhang, Acoustic higher-order topological insulator on a kagome lattice, Nat. Mater. **18**, 108 (2019).
[57] A. El Hassan, F. K. Kunst, A. Moritz, G. Andler, E. J. Bergholtz, and M. Bourennane, Corner states of light in photonic waveguides, Nat. Photonics **13**, 697 (2019).
[58] M. A. J. Herrera, S. N. Kempkes, M. B. de Paz, A. García-Etxarri, I. Swart, C. M. Smith, and D. Bercioux, Corner modes of the breathing kagome lattice: Origin and robustness, Phys. Rev. B **105**, 085411 (2022).
[59] A. Mostafazadeh, Pseudo-Hermiticity versus PT symmetry: The necessary condition for the reality of the spectrum of a non-Hermitian Hamiltonian, J. Math. Phys. (N.Y.) **43**, 205 (2002).
[60] See the Supplemental Material at http://link.aps.org/supplemental/10.1103/PhysRevLett.129.264301 for the realness of the OBC spectrum, extended zero mode in the non-Bloch PT-broken phase, ELCs in different systems, on the robustness issue of the ELC, the effect of dissipation, experimental setup, skin-mode response at the zero mode's eigenfrequency and a supplemental video including the demonstration of the NHSE and the steady-state vibration of the localized and fully extended zero mode, which includes Refs. [26,47,58,61,62].
[61] W. A. Benalcazar and A. Cerjan, Bound states in the continuum of higher-order topological insulators, Phys. Rev. B **101**, 161116(R) (2020).
[62] K. Ding, G. Ma, M. Xiao, Z. Q. Zhang, and C. T. Chan, Emergence, Coalescence, and Topological Properties of Multiple Exceptional Points and Their Experimental Realization, Phys. Rev. X **6**, 021007 (2016).
[63] W. D. Heiss, The physics of exceptional points, J. Phys. A **45**, 444016 (2012).
[64] S. Weigert, Completeness and orthonormality in *PT*-symmetric quantum systems, Phys. Rev. A **68**, 062111 (2003).
[65] D. C. Brody, Biorthogonal quantum mechanics, J. Phys. A **47**, 035305 (2014).
[66] S. Longhi, D. Gatti, and G. D. Valle, Robust light transport in non-Hermitian photonic lattices, Sci. Rep. **5**, 13376 (2015).
[67] F. Song, S. Yao, and Z. Wang, Non-Hermitian Topological Invariants in Real Space, Phys. Rev. Lett. **123**, 246801 (2019).
[68] M.-S. Hwang, H.-C. Lee, K.-H. Kim, K.-Y. Jeong, S.-H. Kwon, K. Koshelev, Y. Kivshar, and H.-G. Park, Ultralow-threshold laser using super-bound states in the continuum, Nat. Commun. **12**, 4135 (2021).
[69] F. Couny, F. Benabid, P. J. Roberts, P. S. Light, and M. G. Raymer, Generation and photonic guidance of multi-octave optical-frequency combs, Science **318**, 1118 (2007).